JOURNAL OF AIRCRAFT
Vol. 31, No. 5, Sept.–Oct. 1994

Using Adaptive Structures to Attenuate Rotary Wing Aeroelastic Response

Fred Nitzsche*
DLR Institute of Aeroelasticity, D-37073 Göttingen, Germany
and
Elmar J. Breitbach†
DLR Institute of Structural Mechanics, D-38108 Braunschweig, Germany

This article investigates the feasibility of employing adaptive material to build both sensors and actuators to attenuate the higher harmonic loads developed at the helicopter rotor blades using the individual blade control (IBC) concept. Both the first elastic flatwise bending (second for hingeless rotors) and the first elastic torsion modes of a single blade deserve special attention in the vibration control. Theoretical investigations, supported by wind-tunnel and flight tests, confirmed that these modes are responsible for the larger amplitude loads at 3/rev in four-blade hingeless rotors. This is a situation for which IBC, based on a collocated actuator-sensor arrangement along the blade, and tailored to act specifically on the bending and the torsion modes, is expected to bring further improvements to the reduction of the overall dynamic response of rotary wings. The results indicate that there are already real situations for which the adaptive material has enough power to accomplish the task without saturation of the applied electrical field.

Nomenclature

B_0, B_1 = boundary condition matrices, $r/R = 0$, $r/R = 1$
$\boldsymbol{b}_0$, $\boldsymbol{b}_1$ = boundary condition vectors, $r/R = 0$, $r/R = 1$
C_T = thrust coefficient, thrust/$(\rho A\Omega^2 R^2)$
c = blade chord
c_θ = blade pitch-control spring constant
D = differentiating matrix
D^*_{ij} = structure compliance coefficients
d_a = distance between layers of piezoelectric actuators
E^* = saturation electric field
E_3 = applied electric field
EI, GJ = blade section bending, torsion rigidities
e_{3x}, e_{3s} = piezoelectric stress coefficients per unit of charge (global axis)
F_W, M_θ = aerodynamic running lift, pitch moment
H = blade section shear resultant
h_s = distance of piezolamina midplane from the blade midplane (positive up)
I_b = total moment of inertia of blade in flapping
i = electric current through piezoelectrodes
$[\,]_i$ = $i \times i$ square matrix
$[\,]_{i\times j}$ = $i \times j$ matrix
$\boldsymbol{K}$ = control gain
K = bending-torsion coupling coefficient
k_θ = blade section radius of gyration
L = integrating matrix
M = blade section bending moment
m = blade section running mass
N = rotor number of blades
n = number of discretizing points
P = algebraic solution of Riccati equation
R = rotor radius
r = blade local radius
s = complex eigenvalue
T = blade section tension
t = time
t_a = adaptive material thickness
$\boldsymbol{u}_R$, $\boldsymbol{u}_L$ = right, left eigenvectors
V = forward speed
w = blade section flatwise bending displacement
x_a = chordwise offset of aerodynamic center behind pitch axis
$\boldsymbol{x}$ = complex state vector
α = forward flight rotor angle of attack
β = blade flap angle (positive up)
Γ_θ, Γ_φ = adaptive material actuation coefficients
γ = Lock number, $\rho acR^4/I_b$
$\boldsymbol{\eta}$ = state vector in aeroelastic modal coordinates
θ = blade section torsion angle
ι = dimensionless current, $i/(\Omega c^2 e_{3x})$
κ = GJ/EI
Λ = matrix of complex eigenvalues
λ = dynamic inflow perturbation
μ = rotor advance ratio, $V/\Omega R$
ν = rotational parameter, $m_R\Omega^2 R^4/(EI)_R$
ρ = air density
σ = weighting number for control synthesis
τ = blade section torque
Φ_R, Φ_L = right, left modal matrices
ϕ, Θ = effective width of adaptive material in bending, torsion
φ = blade section bending slope
ψ = blade azimuth angle, Ωt
Ω = blade rotational frequency
ω_λ = dynamic inflow characteristic frequency
$\mathbf{1}$ = unit matrix (vector)
$\mathbf{0}$ = null matrix (vector)

Subscripts
a = actuator
R = reference quantity
s = sensor

Presented as Paper 92-2452 at the AIAA/ASME/AHS/ASC 33rd Structures, Structural Dynamics, and Materials Conference, Dallas, TX, April 13–15, 1992; received July 20, 1992; revision received Aug. 12, 1993; accepted for publication Jan. 9, 1994.

*Scientist, Bunsenstrasse 10. Member AIAA.
†Director, Lilienthalplatz 7. Member AIAA.

Superscripts

H = Hermitian transpose
T = transpose
$\dot{}$ = dimensionless time derivative, $\partial/\partial\psi$
$'$ = dimensionless space derivative, $R\partial/\partial r$
$+$ = pseudoinverse
$\backslash$ = diagonal matrix

Introduction

THE aeroelastic problem of rotary wings has been studied extensively. There is a recent overview on this subject written by Friedmann,[1] which contains more than 300 references on the existent literature. In particular, the control of the vibration characteristics of helicopter blades has been a matter of special interest. Among the many sources identified to contribute to the forced dynamic response experienced by the helicopter airframe, the most important ones are the rotor hub reactions induced by the inertial and aerodynamic loads acting on the blades. They have a direct impact on the design of the structural components of the helicopter to the specified strength and fatigue criteria. In steady-state forward flight, due to the "filtering" characteristics of the hub, vibration is mainly characterized by a higher harmonic excitation of the helicopter airframe at the frequencies pN/rev, where p is an arbitrary integer number. This excitation, generated by higher harmonic loading of the blades in the rotating frame, cannot be suppressed easily. In general, the vibration level is low in hover flight and increases with the forward flight, in fact limiting the maximum speed of the aircraft.

The mathematical models used to describe the blade aerodynamics assume that the loads acting on the mth blade in the rotating frame are simple periodic functions of the azimuth angle:

$$\psi_m = \psi + m(2\pi/N) \tag{1}$$

and, hence, the hub reactions are commonly expressed by Fourier series expansions, such as the vertical shear induced at the root of the mth blade:

$$H(0)_m = \sum_{n=-\infty}^{\infty} H_n(0)e^{in\psi_m} \tag{2}$$

Summing over all blades, the total thrust simplifies to

$$T = \sum_{m=1}^{N} H(0)_m = N \sum_{p=-\infty}^{\infty} H_{pN}(0)e^{ipN\psi} \tag{3}$$

since the sum is zero, unless n in Eq. (2) is an integer multiple of the number of blades. Therefore, the forces from all blades in the rotating frame exactly cancel at the hub, except for their pN/rev harmonics that are transmitted into the nonrotating frame. The important assumption that lies behind this simple result is that all blades are identical and subject to the same periodic loading, which is not true if the hub has its own dynamics determined by the helicopter airframe. Due to this inherent coupling between rotor and airframe, special attention has been given to avoid certain range of frequencies during the helicopter design. An alternative is to control the magnitude of excitation loads either by passive or active means.

The different designs that have been suggested for the active control of helicopter blades may be classified in two categories, according to their philosophy. In the first group, the time-dependent pitch control is introduced in the nonrotating frame through the helicopter swashplate. This approach is known as higher harmonic control (HHC). In the second group each blade is individually controlled in the rotating frame. This type of control is called individual blade control (IBC). The HHC has been more amply investigated.[2-14] Promising results were obtained, although some limitations were recognized to exist.

The IBC concept was pioneered by Kretz[15] and Ham.[16] It embodies the control of broadband frequencies, using an actuator attached either to the swashplate or individually to each blade. The signals come from sensors mounted on the blades. The IBC involves feedback loops for each blade in the rotating frame and is more effective if comprised of several subsystems, each controlling a specific mode that contributes significantly to the helicopter vibration performance. For most aircraft, these modes are the blade first flatwise bending (second for hingeless blades) and the blade first torsion, which are recognized to have resonance frequencies in the neighborhood of N/rev. The introduction of IBC through the swashplate is limited by the number of blades.[17] Such a limitation imposed restrictions to the use of IBC, although a wind-tunnel model suggested a number of important applications of the method, namely gust alleviation, lag damping augmentation, stall flutter suppression, and flapping stabilization in forward flight.[17-20] The industry has also considered the realization of IBC control without the need of the swashplate.[21]

HHC or IBC?

Although the HHC method presented good results in reducing the vibration loads at the hub, flight tests have indicated that a similar reduction in the airframe vibration levels (e.g., at the pilot seat) is not always accomplished. A recent paper by Papavassiliou et al.[22] was devoted to study the problem. A complete model, including the airframe modelization as a beam, was developed using symbolic manipulation codes. This model was able to confirm that in the presence of airframe-rotor coupling the conventional HHC method fails to suppress both hub and airframe vibration. This is not an entirely unexpected result if one recalls that the HHC is able to control only the frequencies N/rev and $(N \pm 1)$/rev through the introduction of a single frequency, $\omega_{HH} = N$/rev, exciting the harmonic pitch displacement of the swashplate.

On the other hand, the IBC method is suitable for situations where each blade has its own characteristics. If the control laws are synthesized independently, aiming at minimizing the contribution of the modes of each individual blade to the rotor vibration, the magnitude of the hub reactions in the rotating frame becomes naturally lower. Hence, the loads transmitted into the nonrotating frame will also be lower, regardless of the hub filtering performance at N/rev.

With the advent of the adaptive structure technology, the problem of IBC must be reviewed, since a superior authority over specific modes of the blades without the use of the swashplate is theoretically feasible. Particularly attractive seems to be the application of the new technology to provide full control on the dynamic response characteristics of the aforementioned elastic modes of the blades. Furthermore, as long as the adaptive material may be employed as modal sensors, it is possible to eliminate the accelerometers mounted on the blades, which were a matter of special concern in the past due to problems associated with the modal identification in the rotating frame.[20]

Aeroelastic Applications of Adaptive Structures

Most of the reported research on adaptive structures is related to space applications. Few works were published in recent years involving aeroelastic applications. Among them, Ehlers[24] and Ehlers and Weisshaar[23,25] studied static problems of fixed composite wings. Similar studies were developed independently by Song et al.[26] On dynamic aeroelastic problems, there is an investigation on the control of panel flutter conducted by Scott and Weisshaar[27] and a paper coauthored by Lazarus et al.[28] on the comparative performance of adaptive structures vs aerodynamic control surface deflection, aiming at modal damping augmentation and flutter suppression. In this work, the classical typical section model was employed to perform parametric studies, indicating situations for which the use of adaptive structures is advantageous.

The investigations aiming at rotor vibration control are even more rare. Spangler[29] and Spangler and Hall[30] used piezoelectric crystal actuators (PZT) to change the camber of rotor blade sections. The concept of changing the blade camber to alter the aerodynamic load distribution has been used in another paper, where the idea was explored using hydraulic actuators to introduce warping in the airfoil cross section.[31] Spangler and Hall concluded that an efficient way of introducing the new concepts in rotor blade design was to incorporate a servo tab actuated by piezoelectric beams to the blade airfoil. The tab mechanism adds, however, a further complication to the blade dynamics. A more promising approach to obtain suitable deflections with piezoelectric actuators seems to be followed by Barrett.[32] He suggests the use of "directionally attached piezoelectric crystals" and was able to generate bending-independent twist distributions up to 2 deg in blade specimens at high frequencies. In both works the piezoelectric material was employed only to construct actuators, and the reciprocal property that enables their use as sensors was not explored.

Lee et al.[33,34] and Lee and Moon[35] demonstrated that another class of piezoelectric film material (PVF_2) may be used to construct modal sensors and actuators to achieve critical damping of selected modes of one-dimensional structures.

Actuator Equation

The aim of the present work is to perform a feasibility study in which the evaluation of the order of magnitude of the parameters involved are of more interest than the determination of their actual values. A linear mathematical model of a single rotating blade including only the flatwise bending and torsion degrees of freedom (DOF) was developed. The aeroelastic dimensionless equations are cast in the state-vector form, according to the Hellinger-Reissner-Washizu formulation [Eqs. (4a–4f)]. The dimensionless quantities are defined in Table 1:

$$M' = H + \nu T\varphi \tag{4a}$$
$$H' = \nu m\ddot{w} - F_W \tag{4b}$$
$$\varphi' = M/EI \tag{4c}$$
$$w' = -\varphi \tag{4d}$$
$$\tau' = \nu m k_\theta^2(\theta + \ddot{\theta}) - M_\theta \tag{4e}$$
$$\theta' = GJ\tau \tag{4f}$$

Table 1 Nondimensional parameters definition

Parameter	Adimensionalization	Value
c_θ	$c_\theta R/EI_R$	∞ (Cantilever)
c	c/R	0.0555
d_a	d_a/c	0.08
E_3	$(c/R)^3E_3/E^*$	—
EI	EI_R/EI	1.0
e_{3x}	$e_{3x}E^*/m_R\Omega^2$	0.4272
e_{3s}	$e_{3s}E^*/m_R\Omega^2$	0.1617
F_W	R^3F_W/EI_R	—
GJ	EI_R/GJ	1.756
H	R^2H/EI_R	—
h_s	h_s/c	0.04
I_b	$I_b/(m_RR^3)$	$\frac{1}{3}$
K	K/EI_R	0
k_θ	k_θ/R	0.03
M	RM/EI_R	—
M_θ	R^2M_θ/EI_R	—
m	m/m_R	1.0
r	r/R	—
s	s/Ω	—
T	$T/(m_RR^2)$	—
t_a	t_a/c	0.16
w	w/R	—
x_a	x_a/R	0.00555
τ	$R\tau/EI_R$	—
$\phi_{a,s}$	$\phi_{a,s}/c$	0.8
$\Theta_{a,s}$	$\Theta_{a,s}/c$	0.8

where

$$T = \int_r^1 mr\,dr \tag{5}$$

In order to allow possible structural coupling between bending and torsion, Eqs. (4c) and (4f) are modified:

$$\varphi' = D_{11}^*M + D_{13}^*\tau + \Gamma_\varphi E_3 \tag{4c'}$$
$$\theta' = D_{13}^*M + D_{33}^*\tau + \Gamma_\theta E_3 \tag{4f'}$$

The last terms, due to the adaptive material actuation, are added at this point to formulate the control problem. The coefficients Γ_φ and Γ_θ follow the approximations first introduced by Ehlers[24] and Ehlers and Weisshaar.[25] Here, they are dimensionless quantities defined by

$$\Gamma\varphi = \Delta EI(\kappa e_{3x} + KEIe_{3s})t_a d_a \phi_a \tag{6a}$$
$$\Gamma_\theta = \Delta EI(\kappa KEIe_{3x} + e_{3s})t_a d_a \Theta_a \tag{6b}$$

where

$$\Delta = 1/(\kappa - K^2EI^2) \tag{7}$$

and are dependent upon two functions, $\phi_a(r)$ and $\Theta_a(r)$, which describe the width distribution of the adaptive material along the blade span, aiming at independent bending and torsion actuation, respectively (Fig. 1). These two functions may be optimized eventually to achieve modal control in real designs.

The perturbation loads assumed in this work, F_W and M_θ, are attributed to the blade running lift and pitch moment and are based on a linear, two-dimensional blade section, "quasi-static" aerodynamics. They may be derived following equations presented in Ref. 36. Ignoring the unsteady terms and taking the quasisteady approximation $C(k) = 1$, the blade-section dimensionless lift and pitch moment are, respectively:

$$\begin{bmatrix} F_W \\ M_\theta \end{bmatrix} = \gamma I_b \begin{bmatrix} 1 \\ x_a \end{bmatrix} \left([F_{\dot\beta}\ 0\ 0] \frac{\partial}{\partial\psi} \begin{bmatrix} \varphi \\ \theta \\ \lambda \end{bmatrix} + [F_\beta\ -F_\theta\ -F_\lambda] \begin{bmatrix} \varphi \\ \theta \\ \lambda \end{bmatrix} \right) \tag{8}$$

where

$$F_{\dot\beta} = -(r^2 + \mu r \sin\psi)/2 \tag{9a}$$
$$F_\beta = -(\mu r \cos\psi + \mu^2 \sin\psi\cos\psi)/2 \tag{9b}$$
$$F_\theta = (r^2 + 2\mu r \sin\psi + \mu^2 \sin^2\psi)/2 \tag{9c}$$
$$F_\lambda = -(r + \mu \sin\psi)/2 \tag{9d}$$

The dependence upon the inflow perturbation is conveniently maintained to allow an association between the dis-

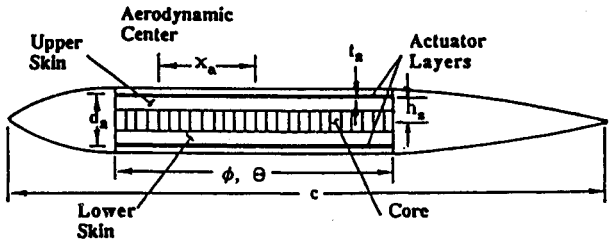

Fig. 1 Blade section definitions.

placement variables and a flight attitude variation like that generated by gusts.

Integration of the Actuator Equation

Equations (4–9) need to be integrated in the independent space variable r. In this article the integrating-matrix method is employed. Integrating matrices have already proved to be an efficient way of systematically integrating systems of ordinary differential equations and formulating eigenvalue problems in structural dynamics. Vakhitov,[37] Hunter,[38] White and Malatino,[39] Murthy,[40] Lehman,[41] and Nitzsche[42] used integrating matrices to obtain numerical solutions for the two-point boundary value problems that appear in aeroelasticity. Hunter chose a displacement variable formulation to solve for the natural lateral vibration characteristics of a cantilevered rotating propeller having nonuniform cross section. Lehman preferred a formulation including both force and displacement variables (state vector formulation) to solve for the aeroelastic characteristics of composite wings. Nitzsche also used the state vector formulation to solve for the aeroelastic characteristics of a vertical axis wind turbine blade, including the flatwise and chordwise bending and torsion DOF. The most interesting advantage of the state vector formulation when using the integrating matrix method is to allow a single-step integration of the differential equations and an easy reduction of the integrated equations either to a standard eigenvalue or to a forced vibration problem in terms of the displacement variables alone.

Appendix A gives a brief review of the integrating matrix scheme. In Appendix B the integration of the actuator equation is performed for a hingeless blade, including the effect of the blade pitch control system flexibility through a nonhomogeneous boundary condition. The problem, in terms of the two essential dependent variables (here chosen to be the flatwise bending slope and the torsion angle), is reduced to the dimensionless equation

$$F\dot{\boldsymbol{x}} + G\boldsymbol{x} = HE_3 \tag{10}$$

$$F = \left[\begin{array}{c|cc} -\gamma I_b L_2 A_1 & L_2 A_2 & [0]_{2n\times 1} \\ [0]_{1\times 2n+1} & [0]_{1\times 2n} & 1/\omega_\lambda^2 \\ \hline 1_{2n+1} & 0_{2n+1} & \end{array}\right] \tag{11}$$

$$G = \left[\begin{array}{c|c} -[\nu^{-1}1_{2n} + L_1 Z \;\; [0]_{2n\times 1}] + \gamma I_b L_2 A_0 & 0_{2n+1} \\ [[0]_{1\times 2n} \qquad -1] & \\ \hline 0_{2n+1} & 1_{2n+1} \end{array}\right] \tag{12}$$

$$H = \left[\begin{array}{c} -L_3\boldsymbol{h} \\ 0 \\ \hline [0]_{2n+1\times 1} \end{array}\right] \tag{13}$$

$$\boldsymbol{x} = [p \quad \dot{p}]^T \tag{14}$$

Here

$$p = [[\varphi]_{1\times n} \quad [\theta]_{1\times n} \quad \lambda]^T \tag{15}$$

and the remaining matrices are defined in Appendix B.

The inflow dynamics is introduced as a simple second-order system [Eq. (16)]. This is a mathematical convenience to avoid a singularity in G. In this study the natural frequency is arbitrarily set to $\omega_\lambda = 10$/rev to make the inflow dynamic response fast enough with respect to the structural modes of interest and the excitation (e.g., gusts) characteristic values:

$$\ddot{\lambda} + \omega_\lambda^2 \lambda = 0 \tag{16}$$

It should be noted that F in Eq. (10) is not invertible due to the nature of the integrating matrix (Appendix A). However, with the exception of the singular value at $\nu = 0$, G is always invertible, as long as Eq. (16) is defined. Furthermore, due to its convenient construction, G is analytically inverted (leaving to the machine a problem of order $2n + 1$, where n is typically 10; this is the only inversion required in the entire process), yielding a slightly different form of the familiar equation:

$$A\dot{\boldsymbol{x}} = \boldsymbol{x} + BE_3 \tag{17}$$

where

$$A = \begin{bmatrix} G_{11}^{-1}F_{11} & G_{11}^{-1}F_{12} \\ \mathbf{1} & \mathbf{0} \end{bmatrix} \tag{18}$$

$$B = \begin{bmatrix} G_{11}^{-1}H_1 \\ \mathbf{0} \end{bmatrix} \tag{19}$$

Since one is interested in performing modal control, Eq. (17) will be transformed next into "aeroelastic" modal coordinates including both aerodynamic and gyroscopic loads. The system has an intrinsic non-Hermitian character. Consequently, the complex eigenvectors are not orthogonal in the normal sense. However, biorthogonality relationships are useful to solve the problem. Neglecting the control loads, the eigenproblem and its adjoint may be formulated in terms of the inverse of the eigenvalues:

$$(A - s^{-1}\mathbf{1})\boldsymbol{u}_R = 0 \tag{20a}$$

$$(A^T - s^{-1}\mathbf{1})\boldsymbol{u}_L = 0 \tag{20b}$$

Here, the right and left eigenvectors of A are ordered in the respective modal matrices, which satisfy the following orthogonality relationships:

$$\Phi_L^H \Phi_R = U_1 = \text{block-diag}\begin{bmatrix} 0 & u_{1_j} \\ u_{1_j}^H & 0 \end{bmatrix} \tag{21a}$$

$$\Phi_L^H A \Phi_R = U_2 = \text{block-diag}\begin{bmatrix} 0 & u_{2_j} \\ u_{2_j}^H & 0 \end{bmatrix} \tag{21b}$$

Both U_1 and U_2 are not diagonal, but block diagonal in the form described in Eqs. (21a) and (21b), with the order of the blocks being 2, and $u_{1_j}/u_{2_j} = s_j$ and $u_{1_j}^H/u_{2_j}^H = s_j^H$ for the jth complex pair of eigenvalues. A similar result was obtained by Meirovitch and Öz[43] when studying flexible spacecraft structures subject to gyroscopic loads. In rotorcraft systems the presence of the aerodynamic loads does not change this property. However

$$U_2^{-1}U_1 = \grave{\Lambda} \tag{22}$$

where $\grave{\Lambda}$ is now the diagonal matrix of eigenvalues. Hence, Eq. (17) may be written as

$$\dot{\boldsymbol{\eta}} = \grave{\Lambda}\boldsymbol{\eta} + \mathcal{B}E_3 \tag{23}$$

with

$$\boldsymbol{x} = \Phi_R \boldsymbol{\eta} \tag{24}$$

$$\mathcal{B} = U_2^{-1}\Phi_L^H B \tag{25}$$

Equation (23) is the desired actuator equation in the aeroelastic modal coordinates. The reciprocal transformation of coordinates, from $\boldsymbol{x}$ to $\boldsymbol{\eta}$, is generally given by the pseudoin-

verse of the modal matrix, here calculated through its single value decomposition:

$$\eta = \Phi_R^{+} x \tag{26}$$

Sensor Equation

Lee and Moon[35] determined that the charge signal measured through the electrodes of a piezoelectric lamina of a laminate plate may be used to derive one-dimensional modal sensors and actuators. Neglecting the transversal deformations, their equation may be adapted to obtain the charge signal developed at a laminate beam subject to both bending and torsion deformations. Taking the time derivative of the charge signal, the current measured at the electrodes of the piezoelectric lamina becomes proportional to the time rate of change of the bending and torsion displacements. Its dimensionless form yields

$$\iota = -h_s \left\{ \int_0^1 \phi_s(r)\dot{\varphi}' \, dr - 2e_{3s}/e_{3x} \int_0^1 \Theta_s(r)\dot{\theta}' \, dr \right\} \tag{27}$$

where $\phi_s(r)$ and $\Theta_s(r)$ are two electrode shape functions, as defined in Lee and Moon's work, here designed to measure both the bending and the torsion velocities. Like their counterparts in the actuator equation developed in a section above, these functions should be optimized to measure individual modal deformations in actual designs of IBC.

Discretizing Eq. (27) and applying the integrating and differentiating matrices presented in Appendix A, the single-output dimensionless sensor equation is obtained

$$\iota = Cx \tag{28}$$

where

$$C = [[0]_{1\times 2n+1} \quad C_2] \tag{29}$$

$$C_2 = -h_s[[\phi_s]_n D \quad -2e_{3s}/e_{3x}[\Theta_s]_n D \quad [0]_{n\times 1}] \tag{30}$$

Using Eq. (24), Eq. (28) may be rewritten in modal coordinates

$$\iota = C\Phi_R \eta = \mathcal{C}\eta \tag{31}$$

Synthesis of a Smart IBC

Assuming that the aeroelastic modal displacements are available for feedback at any instant of time, the control laws will be synthesized using the optimal control theory (LQR algorithm) at selected azimuth angles and different rotor advance ratios. Therefore, Eqs. (9a–9d) are simply evaluated for μ and ψ, and the nonlinear periodic character of the system is simplified. This is not a rigorous approach, but it is assumed to be sufficient for the present analysis. Since measurement noise from piezoelectric sensors can result in degradation of the closed-loop control system, a more robust feedback procedure using the output, as opposed to full-state, was pursued in another work.[44]

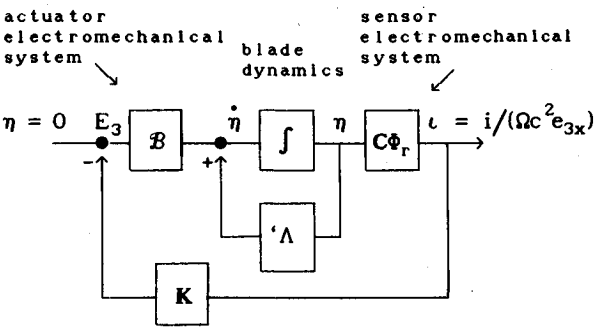

Fig. 2 "Smart" IBC scheme.

The block diagram for the proposed IBC subsystem (controlling an individual elastic mode) is depicted in Fig. 2. The problem is to minimize the cost-function

$$J = \text{expected value} \int_0^\infty [\sigma(\eta^H \grave{Q}\eta) + E_3^2] \, dt \tag{32}$$

subject to Eqs. (23) and (31). As a first step, the sensor equation will not be used to synthesize the control law. Availability of the modal displacement is assumed. This study is useful to evaluate the adaptive material as an actuator, verifying whether it has enough power to attenuate the desired aeroelastic mode. The weighting matrix Q in Eq. (32) is multiplied by the factor σ to ponder the relative costs involved in increasing the damping of the selected aeroelastic modes at the expense of the work done by the adaptive material. The saturation of the adaptive material determines the physical limit of the work. Hence, the general form of Q is a diagonal of zeros, except for the rows associated with the mode (or modes) affected by the control. It is well-known that the solution of this problem is given by the algebraic Riccati equation:

$$P\grave{\Lambda} + \grave{\Lambda}^H P - P\mathcal{B}\mathcal{B}^H P + \sigma Q = 0 \tag{33}$$

In a second step, the complete feedback system will be evaluated, making use of both the actuator and the sensor equations. In this case, the vector of modal displacements in Eq. (32) is substituted for the scalar representing the current through the electrodes of the piezoelectric material; matrix Q collapses to unity and the last term of the Riccati equation needs to be modified [Eq. (34)].

In both situations the control system is a single-input, single-output (SISO), where the input is the voltage E_3, the output is the current ι, and the control law is given by Eq. (35):

$$P\grave{\Lambda} + \grave{\Lambda}^H P - P\mathcal{B}\mathcal{B}^H P + \sigma\mathcal{C}^H\mathcal{C} = 0 \tag{34}$$

$$E_3 = -K\eta = -\mathcal{B}^H P\eta \tag{35}$$

Since the control laws are synthesized in a reduced-order modal space, Φ_R is truncated at the lower modes.

Results

Open-Loop

For the typical helicopter parameters presented in Table 2, the first four complex aeroelastic modes in forward flight [$\mathcal{R}e(s) < 10$/rev] are shown in Fig. 3. They are derived from the first flatwise bending ($1F$), second flatwise bending ($2F$), first torsion ($1T$), and third flatwise bending ($3F$) natural modes of the fixed wing. The evolution of their frequencies and damping ratios with the rotation parameter are presented in Fig. 4. The same two parameters are plotted vs the advance ratio in Fig. 5 and vs the azimuth angle in Fig. 6. It is clear

Table 2 Typical rotor parameters

Parameter	Value	Units
EI_R	6.89×10^4	N·m²
m_R	5.5	kg/m
R	4.926	m
Ω	44.4	rad/s
N	4	—
ρ	1.225	kg/m³
C_T	0.0044	—
γ	5.2	—
ν	100	—
E^* (PZT)	0.381×10^3	V/m

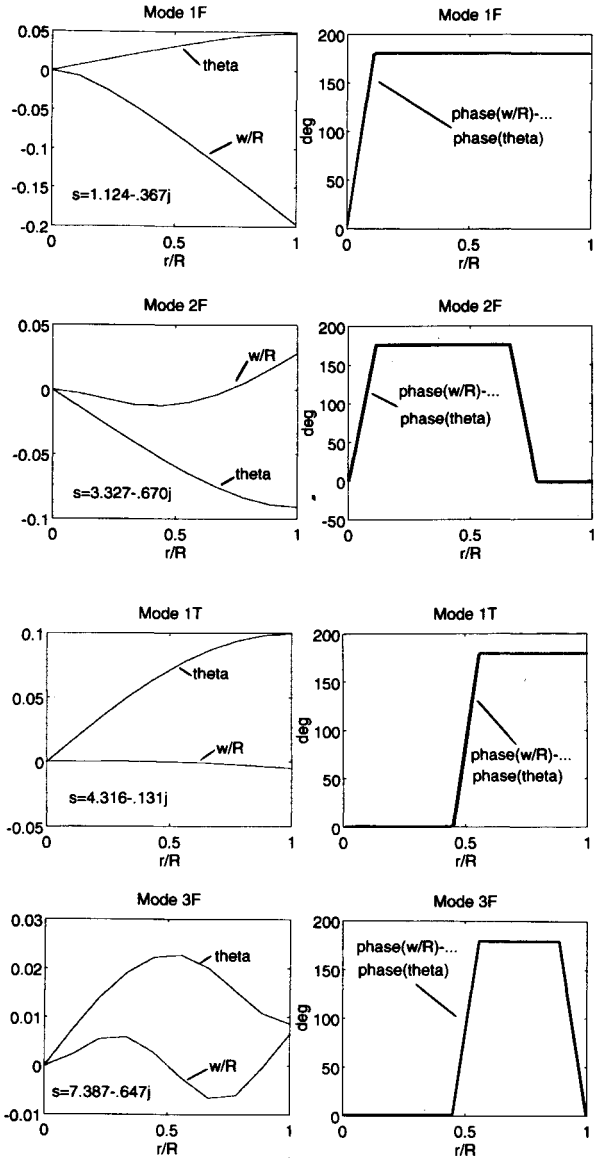

Fig. 3 First four aeroelastic modes for $\mu = 0.1$ and $\psi = 0$: on the left the amplitudes of w and θ; on the right the corresponding phase differences between w and θ. The value of the complex eigenvalues is given in the left figures.

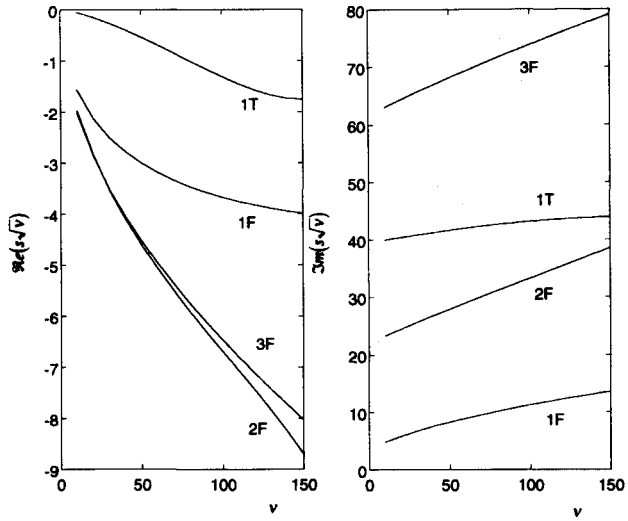

Fig. 4 Evolution of the aeroelastic modes with rotor speed ($\mu = 0.1$, $\psi = 0$).

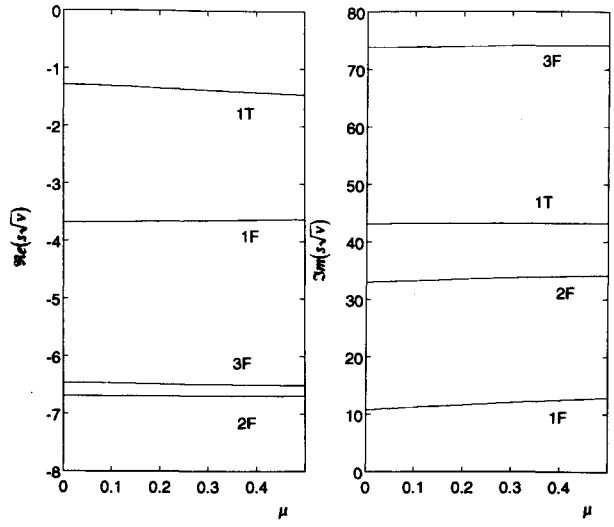

Fig. 5 Evolution of the aeroelastic modes with advance ratio ($\nu = 100$, $\psi = 0$).

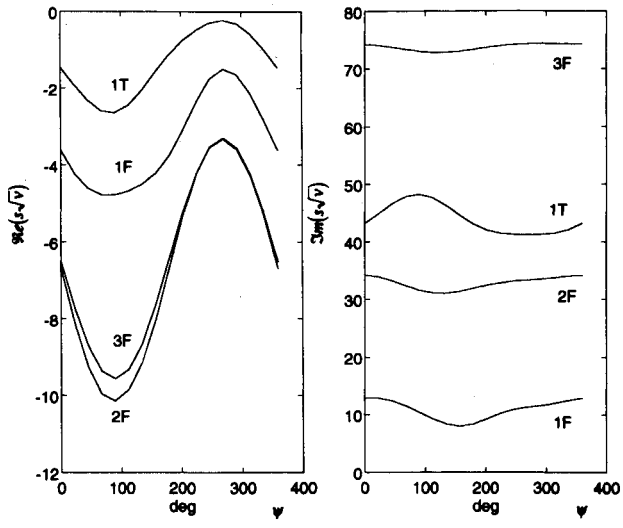

Fig. 6 Evolution of the aeroelastic modes with azimuth angle ($\nu = 100$, $\mu = 0.5$).

that the first torsion mode ($1T$) is the critical one, having almost zero damping ratio at $\mu = 0.5$ and $\psi = 270$ deg.

Closed-Loop

The ability of the adaptive material to provide damping augmentation in characteristic helicopter blades will be first analyzed admitting that the modal coordinates are available for feedback by other means. In other words, the relative participation of the torsion mode in the blade total dynamic response is known in real time.

At the moment, the best candidate for a "smart" actuator is the piezoceramic material (PZT). It has Young's modulus comparable with that of the aluminum and may be embedded in aeronautical structures. Furthermore, its known inability of inducing independent shear deformations may apparently be overcome by providing a partial attachment of the crystal on the substructure through the gluing process.[32] Figure 7 is an example of the result achieved with the technique described in the same reference. Therefore, by gluing the crystals at ± 45 deg on the top and bottom of the substructure, an efficient torsion device may be created.

Next, a control law is sought by the LQR algorithm using the four modes presented in Fig. 3. The 8×8 Q is chosen to select only the $1T$ mode (at 4.12/rev) and its complex conjugate. Figure 8 depicts a plot of the weighting factor against the modal damping of the aforementioned modes. For $\sigma \cong$

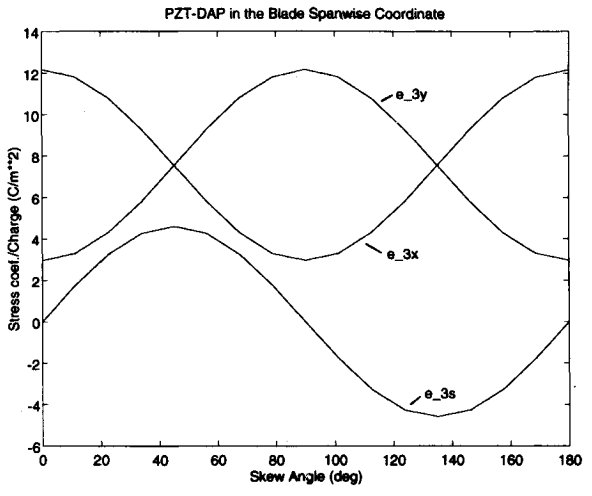

Fig. 7 Stress/charge constant vs skew angle of attachment for PZT using the "directionally attached" concept.[32]

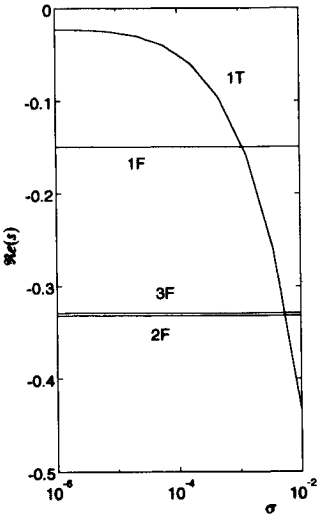

Fig. 8 Control synthesis: weighting factor vs modal damping.

10^{-3}, the damping ratio of $1T$ approaches the one of $1F$ (the remaining modes' damping are kept constant due to the definition of Q). Accepting this value of σ, the complex control law (K_1) yields Eq. (39), indicating that it comprises both a gain (0.0269) and a phase lag (136 deg) with respect to the given azimuth position (270 deg).

To evaluate the effect of the gain on the saturation of the piezoelectric material, a simulation of the closed-loop system in the dimensionless time domain is performed. It is well known that the momentum theory for the forward flight condition gives

$$\lambda = \mu\alpha + C_T/(2\sqrt{\mu^2 + \lambda^2}) \tag{36}$$

Assuming that for one blade $C_T = C_T/N$, Eq. (36) is iteratively evaluated for the initial value $\lambda = C_T/(2N)$ with the data given in Table 2 as a function of α (Fig. 9). Therefore, for $\mu = 0.5$, a perturbation $\Delta\alpha$ in the forward-flight condition around an equilibrium value α_0 causes a variation in the dynamic inflow:

$$\Delta\lambda = \partial\lambda/\partial\alpha|_{\alpha_0}\Delta\alpha \cong 0.0086/\text{deg}\ \Delta\alpha \tag{37}$$

Since the derivative is practically constant, a simple relationship was obtained between the forward-flight perturbation angle (as that generated by a gust) and the initial condition vector x_0. It should be emphasized that $\Delta\lambda = \lambda$ in Eq. (15), as long as in the present formulation all dependent variables

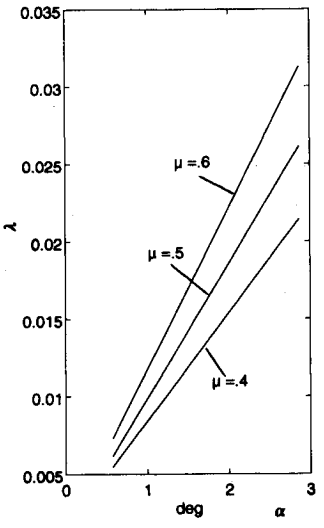

Fig. 9 Dynamic inflow vs rotor attitude angle in forward flight (momentum theory): $C_T = 0.0044$.

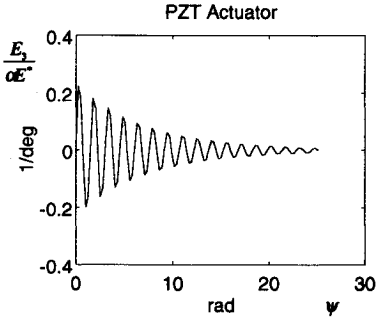

Fig. 10 Applied electrical field vs azimuth angle per degree of flight attitude perturbation. $E_3/E^* = \pm 1$ represent the saturation limits of the material.

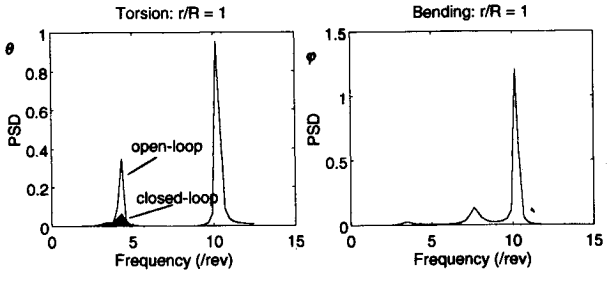

Fig. 11 Power spectral density of the blade torsion and bending slope at the tip: closed- vs open-loop results.

are perturbation quantities. Still assuming that at $t = 0^-$ the system is in equilibrium, a modal displacement initial condition is derived from Eq. (26) per degree of $\Delta\alpha$ [setting $[\varphi]_{1\times n} = [\theta]_{1\times n} = 0$; $\lambda = 1$ in Eq. (15)]:

$$\eta_0 = \Phi_R^+ x_0 \tag{38}$$

The uncontrollable λ modes [Eq. (16)] not included in the control synthesis must be added to provide a proper decomposition of x_0 in the modal space. The control vector is then extended with two additional zeros. Using Eq. (35), a simulation of the control input is plotted in Fig. 10, indicating that $|E_3/E^*| < 1$, and no saturation of the adaptive material is observed. As long as the curve is plotted per degree of $\Delta\alpha$, a perturbation in forward flight condition of up to 4 deg would be acceptable. In Fig. 11 the power spectral density (PSD) of both the torsion angle and the bending slope at the blade tip are presented. It is clear that the performance of the IBC is satisfactory, cutting by a factor of four the torsion response

at 4/rev. No change in the bending slope response can be expected with the chosen Q, but since the amplitude of the two responses are of the same order of magnitude, a significant improvement of the total response of the blade at the critical value of N/rev is indeed verified. The peak at 10/rev is due to the inflow dynamics resonance, arbitrarily taken at this frequency.

The next step is to analyze a closed-loop performance using the adaptive material as a sensor as well. It is obvious that either PZT (with the concept of Ref. 32) or PVF_2 provide suitable sensors, as long as no power requirement exists in this case. The PZT material will deliver higher current output, but PVF_2 may also be employed with current amplifiers. Figures 12–14 are the counterparts of Figs. 8, 10 and 11, respectively, for a complete "smart" IBC using only PZT material. In this case, the control law ($\sigma = 10$) should affect all modes. The system has a full-state feedback character since no attempt was made to optimize ϕ_s and Θ_s in the present work. Comparing the control gain obtained in this case (K_2) with the previous one (K_1), it is evident that the damping ratio of the higher-damped modes cannot be significantly increased by the full-state feedback:

$$K_1,\ K_2 = \begin{bmatrix} 0 \\ 0 \\ 0 \\ 0 \\ 0.0269 \angle 136\ \text{deg} \\ 0.0269 \angle -136\ \text{deg} \\ 0 \\ 0 \end{bmatrix}, \begin{bmatrix} 0.009 \angle -88.3\ \text{deg} \\ 0.009 \angle 88.3\ \text{deg} \\ 0.0012 \angle 72.9\ \text{deg} \\ 0.0012 \angle -72.9\ \text{deg} \\ 0.0265 \angle 134\ \text{deg} \\ 0.0265 \angle -134\ \text{deg} \\ 0.0048 \angle 33.7\ \text{deg} \\ 0.0048 \angle -33.7\ \text{deg} \end{bmatrix} \tag{39}$$

Further inspection of Fig. 12 reveals that for the high to moderate control costs (low σ), which are necessary to avoid saturation of the adaptive material, no modification in the damping ratio of the bending-related modes is verified. In fact, this is an indication that only very lightly loaded modes (with low aerodynamic damping) benefit from the present technology of piezoelectric actuators.

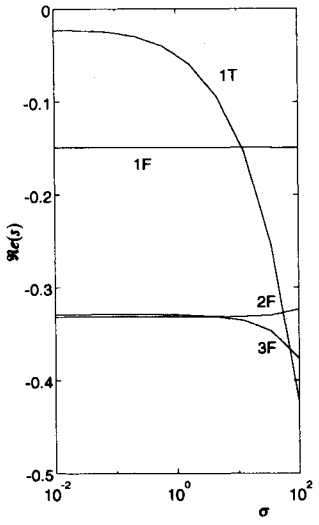

Fig. 12 Control synthesis: weighting factor vs modal damping. "Smart" IBC system.

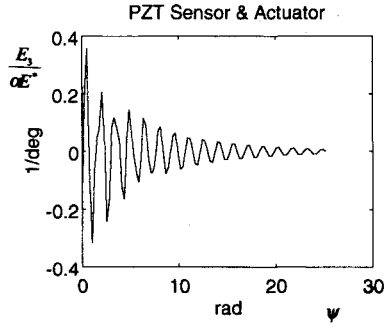

Fig. 13 Applied electrical field versus azimuth angle per degree of flight attitude perturbation. $E_3/E^* = \pm 1$ represent the saturation limits of the material. "Smart" IBC system.

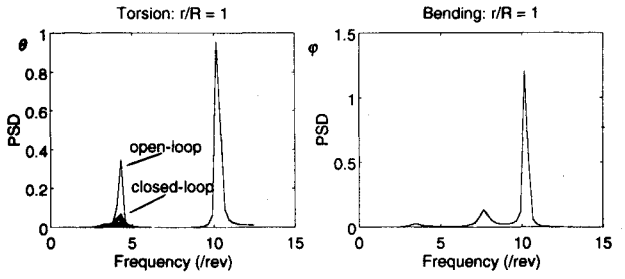

Fig. 14 Power spectral density of the blade torsion and bending slope at the tip: closed- vs open-loop results. "Smart" IBC system.

Conclusions

The main conclusions of this work could be summarized as follows:

1) For low-damped, lightly loaded blade modes in hingeless rotors, adaptive materials in general and piezoceramics in particular already have enough power to provide attenuation in the dynamic response of helicopter blades by the IBC method without reaching the saturation level. A reduction of a factor of four at N/rev was verified for a typical helicopter rotor. Perturbations (due to gusts) up to 4 deg in the forward-flight angle of attack could be tolerated without saturation of the adaptive material.

2) A distributed IBC using a sensor-actuator arrangement may be designed for actual rotors using the optimal control theory assuming an on-line adaptive algorithm dependent on both the advance ratio and the blade azimuth angle.

3) Integrating-differentiating matrices are a powerful tool to deal with problems commonly encountered in the control theory, due to their semianalytical, self-contained compact formulation.

Appendix A: Integrating and Differentiating Matrices

For the sake of completeness, a summary of the integrating-differentiating method used in this article is presented. A better description of the method may be found in Refs. 41 and 42.

Let $f(x)$ be a dimensionless function defined in the interval [0,1]. In addition, suppose that the interval is discretized in n grid points such as $x_1 = 0$ and $x_n = 1$. Assuming that $f(x)$ can be approximated by a mth degree polynomial in the ith subinterval, $[x_i, x_{i+1}]$, with $m \leq n + 1$ and $i = 1, \ldots n - 1$, an integration of $f(x)$ over such a subinterval would appear as

$$\int_{x_i}^{x_{i+1}} f(x) \cong \sum_{k=j}^{k=j+m} \mathcal{W}_{ik} f_k \tag{A1}$$

where $\mathcal{W}_{ik}$ are weighting numbers that are independent of the value of the function. The integer j is the starting point of a general sequence of consecutive $m + 1$ grid points at which the function is approximated by the mth degree polynomial ($1 \leq j \leq n - m$). Defining the vectors

$$\mathcal{F} = \left[0,\ \int_{x_1}^{x_2} f(x)\,dx, \ldots \int_{x_{n-1}}^{x_n} f(x)\,dx\right]^T_{n\times 1} \tag{A2}$$

$$f = [f_1 f_2 \ldots f_n]^T_{n\times 1} \tag{A3}$$

the integral of Eq. (A1) can be expressed for all subintervals in a matrix notation

$$\mathcal{F} = \mathcal{W}_m \boldsymbol{f} \tag{A4}$$

where m denotes the degree of the approximating polynomial. $\mathcal{W}_m$ is a $n \times n$ weighting matrix whose first row is zero as long as the first element of $\mathcal{F}$ is zero. A sequence of integrals

$$\mathcal{F}_s = \left[0, \int_{x_1}^{x_2} f(x)\,dx, \ldots \int_{x_1}^{x_n} f(x)\,dx\right]^T_{n\times 1} \tag{A5}$$

would be represented by

$$\mathcal{F}_s = S_n \mathcal{W}_m \boldsymbol{f} \tag{A6}$$

where S_n is a $n \times n$ lower triangular summing matrix for which $S_{ij} = 1$ when $i \geq j$ and $S_{ij} = 0$ if $i < j$. The integrating matrix is then defined as the linear operator

$$L = S_n \mathcal{W}_m \tag{A7}$$

with the property

$$\boldsymbol{f} = L\boldsymbol{f}' + f(0)[1]_{n\times 1} \tag{A8}$$

where the boundary condition vector remains to be evaluated. It is worthwhile to mention that due to the row of zeros in $\mathcal{W}_m$ the integrating matrix is singular. Furthermore, it is not symmetric. Two boundary-condition vector operators

$$\boldsymbol{b}_0 = [1 \quad 0, \ldots, 0], \qquad \boldsymbol{b}_1 = [0 \quad 0, \ldots, 1] \tag{A9}$$

and their matrix correspondents, $B_{0,1} = [1]_{n\times 1}\boldsymbol{b}_{0,1}$, provide a series of properties that are useful in the solution of two-point boundary value problems (Table A1).

Given a differential equation

$$\boldsymbol{y}' = A\boldsymbol{y} + \boldsymbol{b} \tag{A10}$$

where $\boldsymbol{y}$ is a vector of N dependent variables, $y_1, \ldots, y_N$, a discrete version of Eq. (A10) is formally obtained

$$\begin{bmatrix} [y_1]_{n\times 1} \\ [y_2]_{n\times 1} \\ \vdots \\ [y_N]_{n\times 1} \end{bmatrix}' = \begin{bmatrix} [\tilde{A}_{11}]_n & [\tilde{A}_{12}]_n & \cdots \\ [\tilde{A}_{21}]_n & \cdots & \\ \vdots & & \\ [\tilde{A}_{N1}]_n & \cdots & \end{bmatrix} \tilde{\boldsymbol{y}} + \begin{bmatrix} [b_1]_{n\times 1} \\ [b_2]_{n\times 1} \\ \vdots \\ [b_N]_{n\times 1} \end{bmatrix} \tag{A11}$$

or shortly, $\tilde{\boldsymbol{y}} = \tilde{A}\tilde{\boldsymbol{y}} + \tilde{\boldsymbol{b}}$, and next multiplied by the extended integrating matrix operator:

$$\tilde{L} = \text{block-diag } L \tag{A12}$$

yielding

$$\tilde{\boldsymbol{y}} = \tilde{L}\tilde{A}\tilde{\boldsymbol{y}} + \tilde{L}\tilde{\boldsymbol{b}} + \tilde{\boldsymbol{k}} \tag{A13}$$

As a final step, Eq. (A13) is solved for $\tilde{\boldsymbol{k}}$ using the boundary conditions and properties given in Table A1. Since it is generally necessary to apply different types of boundary conditions at $x = 0$ and $x = 1$, it would be formally required to premultiply Eq. (A13) by block-diagonal boundary condition matrices $\tilde{B}_0$ and $\tilde{B}_1$, respectively. However, if the problem is cast in its state vector form, the matrix A is always sparse, and the system can be easily split into N first-order subsystems for which the determination of $\tilde{\boldsymbol{k}}$ is rather simplified. This procedure will be discussed in Appendix B in connection with the present problem. A compendium with the numerical form of the most common integrating matrices may be found in Refs. 38 and 41.

Table A1 Boundary-condition matrices properties

$B_0 L = 0$	$B_1 L = \int_0^1 f\,dx$
$B_0 \boldsymbol{f} = f_0 = f(0)[1]_{n\times 1}$	$B_1 \boldsymbol{f} = f_1 = f(1)[1]_{n\times 1}$
$B_0 \boldsymbol{k} = \boldsymbol{k}$	$B_1 \boldsymbol{k} = \boldsymbol{k}$

Differentiating matrices can also be derived. The Newton forward and backward formulas presented in Abramovitz and Stegun's[45] handbook are useful to generate $n \times n$ differentiating matrices, which are compatible with the mth degree polynomial used in the integrating matrix and perform the reciprocal operation: $\boldsymbol{f}' = D\boldsymbol{f}$.

Appendix B: Actuator Equation: Hingeless Blade

Equations (4–9) will be integrated by the integrating matrix method. These steps are followed:

Step 1. Discretize and apply the L operator:

$$[M]_{n\times 1} = L[H]_{n\times 1} + \nu L[\check{T}]_n[\varphi]_{n\times 1} + \boldsymbol{k}_M \tag{B1a}$$

$$[H]_{n\times 1} = \nu L[\check{m}]_n[\ddot{w}]_{n\times 1} - L[F_W]_{n\times 1} + \boldsymbol{k}_H \tag{B1b}$$

$$[\varphi]_{n\times 1} = L[\check{D}^*_{11}]_n[M]_{n\times 1} + L[\check{D}^*_{13}]_n[\tau]_{n\times 1} + L[\Gamma_\varphi]_{n\times 1}E_3 + \boldsymbol{k}_\varphi \tag{B1c}$$

$$[w]_{n\times 1} = -L[\varphi]_{n\times 1} + \boldsymbol{k}_W \tag{B1d}$$

$$[\tau]_{n\times 1} = \nu L[\check{m}k^2_\theta]_n([\ddot{\theta}]_{n\times 1} + [\theta]_{n\times 1}) - L[M_\theta]_{n\times 1} + \boldsymbol{k}_\tau \tag{B1e}$$

$$[\theta]_{n\times 1} = L[\check{D}^*_{13}]_n[M]_{n\times 1} + L[\check{D}^*_{33}]_n[\tau]_{n\times 1} + L[\Gamma_\theta]_{n\times 1}E_3 + \boldsymbol{k}_\theta \tag{B1f}$$

where

$$[T]_{n\times 1} = (B_1 - \mathbf{1})L[\check{m}]_n[r]_{n\times 1} \tag{B2}$$

$$[D^*_{11}]_{n\times 1} = [EI(1 + K^2EI^2\Delta)]_{n\times 1} \tag{B3a}$$

$$[D^*_{13}]_{n\times 1} = [KEI^2\Delta]_{n\times 1} \tag{B3b}$$

$$[D^*_{33}]_{n\times 1} = [EI\Delta]_{n\times 1} \tag{B3c}$$

$$[\Delta]_{n\times 1} = [1/(\kappa - K^2EI^2)]_{n\times 1} \tag{B3d}$$

Step 2. Use boundary conditions to determine constants of integration:

$$\varphi(0) = 0 \Rightarrow \boldsymbol{k}_\varphi = 0 \tag{B4a}$$

$$w(0) = 0 \Rightarrow \boldsymbol{k}_w = 0 \tag{B4b}$$

$$M(1) = 0 \Rightarrow \boldsymbol{k}_M = -B_1L[H]_{n\times 1} - \nu B_1L[\check{T}]_n[\varphi]_{n\times 1} \tag{B4c}$$

$$H(1) = 0 \Rightarrow \boldsymbol{k}_H = -\nu B_1L[\check{m}]_n[\ddot{w}]_{n\times 1} + B_1L[F_W]_{n\times 1} \tag{B4d}$$

$$\tau(1) = 0 \Rightarrow \boldsymbol{k}_\tau = -\nu B_1L[\check{m}k^2_\theta]_n([\ddot{\theta}]_{n\times 1} + [\theta]_{n\times 1}) + B_1L[M_\theta]_{n\times 1} \tag{B4e}$$

$$\tau(0) = c_\theta\theta(0) \Rightarrow \boldsymbol{k}_\theta = (1/c_\theta)\boldsymbol{k}_\tau \tag{B4f}$$

Equation (B4f) is a nonhomogeneous boundary condition associated with the blade rigid body mode, due to the pitch control flexibility. If $c_\theta \to \infty$, a perfect cantilever blade is obtained.

Step 3. Substitute Eqs. (B4a–4f) into Eqs. (B1a–1f) and solve for the essential dependent variables, here chosen as $[\varphi]$ and $[\theta]$. The size of the global matrix is reduced at the expense of the number of matrix multiplications:

$$(\mathbf{1} + \nu L_1Z)\boldsymbol{q} = L_2[-\nu A_2\ddot{\boldsymbol{q}} + \nu\gamma I_b(A_1\dot{\boldsymbol{p}} + A_0\boldsymbol{p})] + \nu L_3\boldsymbol{h}E_3 \tag{B5}$$

where

$$q = \begin{bmatrix} [\varphi]_{n\times 1} \\ [\theta]_{n\times 1} \end{bmatrix} \tag{B6}$$

$$p = \begin{bmatrix} q \\ \lambda \end{bmatrix} \tag{B7}$$

$$h = \begin{bmatrix} [\Gamma_\varphi]_{n\times 1} \\ [\Gamma_\theta]_{n\times 1} \end{bmatrix} \tag{B8}$$

$$Z = \begin{bmatrix} [\breve{T}]_n & \\ & [\breve{m}k_\theta^2]_n \end{bmatrix} \tag{B9}$$

$$A_2 = \begin{bmatrix} [\breve{m}]_n L & \\ & [\breve{m}k_\theta^2]_n \end{bmatrix} \tag{B10}$$

$$A_1 = \begin{bmatrix} 1_n \\ [\breve{x}_a]_n \end{bmatrix} [[\breve{F}_\beta]_n \quad 0_n \quad 0_{n\times 1}] \tag{B11}$$

$$A_0 = \begin{bmatrix} 1_n \\ [\breve{x}_a]_n \end{bmatrix} [[\breve{F}_\beta]_n \quad -[\breve{F}_\theta]_n \quad -[\breve{F}_\lambda]_{n\times 1}] \tag{B12}$$

$$L_1 = \begin{bmatrix} L[\breve{D}_{11}^*]_n L_c & L[\breve{D}_{13}^*]_n L_c \\ L[\breve{D}_{13}^*]_n L_c & L_{nh} \end{bmatrix} \tag{B13}$$

$$L_2 = \begin{bmatrix} L[\breve{D}_{11}^*]_n L_c^2 & L[\breve{D}_{13}^*]_n L_c \\ L[\breve{D}_{13}^*]_n L_c^2 & L_{nh} \end{bmatrix} \tag{B14}$$

$$L_3 = \begin{bmatrix} L & \\ & L \end{bmatrix} \tag{B15}$$

with two "special" boundary condition matrices

$$L_c = (B_1 - \mathbf{1})L = \int_r^1 [\breve{\ }]\, dr \tag{B16}$$

$$L_{nh} = L[\breve{D}_{33}^*]_n L_c + (1/c_\theta) B_1 L \tag{B17}$$

associated with the "cantilever" bending and the "nonhomogeneous torsion" conditions, respectively.

References

[1]Friedmann, P. P., "Rotary-Wing Aeroelasticity with Application to VTOL Vehicles," *Proceedings of the AIAA/ASME/ASCE/AHS/ASC 31st Structures, Structural Dynamics, and Materials Conference*, Pt. 3, AIAA, Washington, DC, 1990, pp. 1624–1670.

[2]Johnson, W., "Self-Tuning Regulators for Multicyclic Control of Helicopter Vibrations," NASA TP-1996, March 1982.

[3]Molusis, J. A., Hammond, C. E., and Cline J. H., "A Unified Approach to the Optimal Design of Adaptive and Gain Scheduled Controllers to Achieve Minimum Helicopter Vibration," *Journal of the American Helicopter Society*, Vol. 28, No. 2, 1983, pp. 9–18.

[4]Hammond, C. E., "Wind Tunnel Results Showing Rotor Vibration Loads Reduction Using Higher Harmonic Blade Pitch," *Journal of the American Helicopter Society*, Vol. 28, No. 1, 1983, pp. 10–15.

[5]Davis, M. W., "Refinement and Evaluation of Helicopter Real-Time Self-Adaptive Active Vibration Control Algorithms," NASA CR-3821, Aug. 1984.

[6]Wood, E. R., Powers, R., Cline, J. H., and Hammond, C. E., "On Developing and Flight Testing a Higher Harmonic Control System," *Journal of the American Helicopter Society*, Vol. 30, No. 1, 1985, pp. 3–20.

[7]Achacte, M., and Polychroniadis, M., "Development of an Experimental System for Active Control of Vibrations in Helicopters—Development Methodology for an Airborne System," *Vertica*, Vol. 11, Nos. 1/2, 1987, pp. 123–138.

[8]Shaw, J., Albion, N., Hanker, E. J., and Teal, R. S., "Higher Harmonic Control: Wind Tunnel Demonstration of Fully Effective Vibratory Hub Force Suppression," *Journal of the American Helicopter Society*, Vol. 34, No. 1, 1989, pp. 14–25.

[9]Chopra, I., and McCloud, J. L., "A Numerical Simulation Study of Open-Loop, Closed-Loop and Adaptive Multicyclic Control Systems," *Journal of the American Helicopter Society*, Vol. 28, No. 1, 1983, pp. 63–77.

[10]Jacob, H. G., and Lehmann, G., "Optimization of Blade Pitch Angle for Higher Harmonic Rotor Control," *Vertica*, Vol. 7, No. 3, 1983, pp. 271–286.

[11]Nguyen, K., and Chopra, I., "Application of Higher Harmonic Control (HHC) to Hingeless Rotor Systems," *Proceedings of the AIAA/ASME/ASCE/AHS/ASC 30th Structures, Structural Dynamics, and Materials Conference*, Pt. 1, AIAA, Washington, DC, 1989, pp. 507–520.

[12]Lehmann, G., "The Effect of Higher Harmonic Control (HHC) on a Four-Bladed Hingeless Model Rotor," *Vertica*, Vol. 9, No. 3, 1985, pp. 273–284.

[13]Robinson, L. H., and Friedmann, P. P., "Analytical Simulation of Higher Harmonic Control Using a New Aeroelastic Model," *Proceedings of the AIAA/ASME/ASCE/AHS/ASC 30th Structures, Structural Dynamics, and Materials Conference*, Pt. 3, AIAA, Washington, DC, 1989, pp. 1394–1406.

[14]Kube, R., "Aeroelastic Effects of Helicopter Vibration Reduction by Higher Harmonic Control," *Proceedings of the International Forum on Aeroelasticity and Structural Dynamics 1991*, German Society for Aeronautics and Astronautics (DGLR), Bonn, Germany, 1991, pp. 496–504.

[15]Kretz, M., "Research in Multicyclic and Active Control of Rotary Wings," *Vertica*, Vol. 1, Nos. 1/2, 1976, pp. 95–105.

[16]Ham, N. D., "Helicopter Individual-Blade-Control Research at MIT 1977–1985," *Vertica*, Vol. 11, Nos. 1/2, 1987, pp. 109–122.

[17]Ham, N. D., "A Simple System for Helicopter Individual-Blade-Control and Its Application to Gust Alleviation," 6th European Rotorcraft Forum, Paper 70, Bristol, England, UK, Sept. 1980.

[18]Ham, N. D., "Helicopter Gust Alleviation, Attitude Stabilization and Vibration Alleviation Using Individual Blade Control Through a Conventional Swashplate," 11th European Rotorcraft Forum, Paper 75, London, Sept. 1985.

[19]Ham, N. D., Behal, B. L., and McKillip, R. M., "Helicopter Rotor Lag Damping Augmentation Through Individual-Blade-Control," *Vertica*, Vol. 7, No. 4, 1983, pp. 361–371.

[20]McKillip, R. M., "Periodic Control of the Individual-Blade-Control Helicopter Rotor," *Vertica*, Vol. 9, No. 2, 1985, pp. 199–225.

[21]Guinn, K. F., "Individual Blade Control Independent of the Swashplate," *Journal of the American Helicopter Society*, Vol. 27, No. 3, 1982, pp. 25–31.

[22]Papavassiliou, I., Friedmann, P. P., and Venkatesan, C., "Coupled Rotor-Flexible Fuselage Vibration Reduction Using Open-Loop Higher Harmonic Control," *Proceedings of the AIAA/ASME/ASCE/AHS/ASC 32nd Structures, Structural Dynamics, and Materials Conference*, Pt. 3, AIAA, Washington, DC, 1991, pp. 2011–2035.

[23]Ehlers, S. M., and Weisshaar, T. A., "Static Aeroelastic Behavior of an Adaptive Laminated Piezoelectric Composite Wing," *Proceedings of the AIAA/ASME/ASCE/AHS/ASC 31st Structures, Structural Dynamics, and Materials Conference*, Pt. 3, AIAA, Washington, DC, 1990, pp. 1611–1623.

[24]Ehlers, S. M., "Aeroelastic Behavior of an Adaptive Lifting Surface," Ph.D. Dissertation, School of Aeronautics and Astronautics, Purdue Univ., West Lafayette, IN, May 1991.

[25]Ehlers, S. M., and Weisshaar, T. A., "Adaptive Static and Dynamic Aeroelastic Design," Workshop on Smart Material Systems and Structures, German Society for Aeronautics and Astronautics (DGLR), Bonn, Germany, 1991, pp. 65–75.

[26]Song, O., Librescu, L., and Rogers, C. A., "Static Aeroelastic Behavior of Adaptive Aircraft Wing Structures Modeled as Composite Thin-Walled Beams," *Workshop on Smart Material Systems and Structures*, German Society for Aeronautics and Astronautics (DGLR), Bonn, Germany, 1991, pp. 46–55.

[27]Scott, R. C., and Weisshaar, T. A., "Controlling Panel Flutter Using Adaptive Materials," *Proceedings of the AIAA/ASME/ASCE/AHS/ASC 32nd Structures, Structural Dynamics, and Materials Conference*, Pt. 3, AIAA, Washington, DC, 1991, pp. 2218–2229.

[28]Lazarus, K. B., Crawley, E. F., and Lin, C. Y., "Fundamental Mechanisms of Aeroelastic Control with Control Surface and Strain Actuation," *Proceedings of the AIAA/ASME/ASCE/AHS/ASC 32nd Structures, Structural Dynamics, and Materials Conference*, Pt. 3, AIAA, Washington, DC, 1991, pp. 1817–1831.

[29]Spangler, R. L., Jr., "Piezoelectric Actuators for Helicopter Rotor Control," M.S. Thesis, M.I.T., Cambridge, MA, Jan. 1989.

[30]Spangler, R. L., Jr., and Hall, S. R., "Piezoelectric Actuators for Helicopter Rotor Control," *Proceedings of the AIAA/ASME/ASCE/AHS/ASC 31st Structures, Structural Dynamics, and Materials Conference*, Pt. 3, AIAA, Washington, DC, 1990, pp. 1589–1599.

[31]Kurhorst, S., and Oery, H., "Active Twist Control of a Wind Tunnel Model Wing," *Workshop on Smart Material Systems and Structures*, German Society for Aeronautics and Astronautics (DGLR), Bonn, Germany, 1991, pp. 76–83.

[32]Barrett, R., "Intelligent Rotor Blade Actuation Through Directionally Attached Piezoelectric Crystals," M.S. Thesis, Dept. of Aerospace Engineering, Univ. of Maryland, College Park, MD, 1991.

[33]Lee, C.-K., Chiang, W.-W, and O'Sullivan, T. C., "Piezoelectric Modal Sensors and Actuators Achieving Critical Active Damping on a Cantilever Plate," *Proceedings of the AIAA/ASME/ASCE/AHS/ASC 30th Structures, Structural Dynamics, and Materials Conference*, Pt. 4, AIAA, Washington, DC, 1989, pp. 2018–2026.

[34]Lee, C.-K., O'Sullivan, T. C., and Chiang, W.-W., "Piezoelectric Strain Rate Sensor and Actuator Designs for Active Vibration Control," *Proceedings of the AIAA/ASME/ASCE/AHS/ASC 32nd Structures, Structural Dynamics, and Materials Conference*, Pt. 3, AIAA, Washington, DC, 1991, pp. 2197–2207.

[35]Lee, C.-K., and Moon, F. C., "Modal Sensors/Actuators," *Journal of Applied Mechanics*, Vol. 57, June 1990, pp. 434–441.

[36]Johnson, W., *Helicopter Theory*, Princeton Univ. Press, Princeton, NJ, 1980, pp. 548–600.

[37]Vakhitov, M. B., "Integrating Matrices as a Means of Numerical Solution of Differential Equations in Structural Mechanics," *Soviet Aeronautics*, Vol. 9, No. 3, 1966, pp. 27–33.

[38]Hunter, W. F., "Integrating Matrix Method for Determining the Natural Vibration Characteristics of Propeller Blades," NASA TN D-6064, Dec. 1970.

[39]White, W. F., Jr., and Malatino, R. E., "A Numerical Method for Determining the Natural Vibration Characteristics of Rotating Nonuniform Cantilever Blades," NASA TM X-72751, Oct. 1975.

[40]Murthy, V. R., "Dynamic Characteristics of Rotor Blades: Integrating Matrix Method," *AIAA Journal*, Vol. 15, No. 4, 1977, pp. 595–597.

[41]Lehman, L. L., "Hybrid State Vector Methods for Structural Dynamic and Aeroelastic Boundary Value Problems," NASA CR-3591, Aug. 1982.

[42]Nitzsche, F., "Aeroelastic Analysis of a Darrieus Type Wind Turbine Blade with Troposkien Geometry," Ph.D. Dissertation, Stanford Univ., Stanford, CA, June 1983.

[43]Meirovitch, L., and Öz, H., "Modal-Space Control of Distributed Gyroscopic Systems," *Journal of Guidance and Control*, Vol. 3, No. 2, 1980, pp. 140–150.

[44]Nitzsche, F., and Breitbach, E., "The Smart Structures Technology in the Vibration Control of Helicopter Blades in Forward Flight," *Proceedings of the 1st European Conference on Smart Structures and Materials*, Inst. of Physics Publishing, Bristol, England, UK, 1992, pp. 321–324.

[45]Abramovitz, M., and Stegun, I. A. (ed.), *Handbook of Mathematical Functions*, Dover, New York, 1970, pp. 877–899.